Journal of Solid State Chemistry 184 (2011) 502–508

Contents lists available at ScienceDirect

Journal of Solid State Chemistry

journal homepage: www.elsevier.com/locate/jssc

Preparation and photocatalytic activity of Sb_2S_3/Bi_2S_3 doped TiO_2 from complex precursor via gel–hydrothermal treatment

Yan Huang, Gang Xie*, Sanping Chen*, Shengli Gao*

Key Laboratory of Synthetic and Natural Functional Molecule Chemistry of Ministry of Education, College of Chemistry & Materials Science, Northwest University, Xi'an 710069, People's Republic of China

ARTICLE INFO

Article history:
Received 28 September 2010
Received in revised form
1 December 2010
Accepted 6 December 2010
Available online 19 December 2010

Keywords:
Sb_2S_3/Bi_2S_3 doped TiO_2
Coordination compound precursor
Gel–hydrothermal route
Photocatalytic activity

ABSTRACT

Sb_2S_3/Bi_2S_3 doped TiO_2 were prepared with the coordination compounds $[M(S_2CNEt)_3]$ (M=Sb, Bi; S_2CNEt=pyrrolidinedithiocarbamate) as precursors via gel–hydrothermal techniques. The doped TiO_2 were characterized by XRD, SEM, XPS and UV–vis diffuse reflectance means. The photocatalyst based on doped TiO_2 for photodecolorization of 4-nitrophenol (4-NP) was examined. The optimal Bi_2S_3/Sb_2S_3 content, pH and different doped techniques have been investigated. Photocatalytic tests reveal that M_2S_3 doped TiO_2 via the gel–hydrothermal route performs better photocatalytic activity for photodegradation reaction of 4-nitrophenol (4-NP).

1. Introduction

As the representative semiconductor oxide, titanium dioxide (TiO_2) has attracted intense attention for its technologically important application in photoelectrochemical process, dye-sensitized solar cell and photocatalysis. Recently, substantial effort has been devoted to using metal and nonmetal doping strategies to impart TiO_2 with active photocatalytic performance in response to growing environmental concerns [1–17]. The doping process improves TiO_2 photocatalytic activity through increasing the concentration of charge carrier, curtailing the band gap, or changing the equilibrium concentration of electrons or holes [18–21]. Sb or Bi doped TiO_2 photocatalysts in previous works were active for photodegradation of pollutants in waste water [22–25]. The heterosystem of their sulfureteds Sb_2S_3/TiO_2 and Bi_2S_3/TiO_2 [26,27] showed a much higher photocatalytic activity than bare TiO_2 or Bi_2S_3 illuminated by visible light [28]. The doped TiO_2 demonstrates a high ability to degrade organic dyes in visible light and UV–vis light. However, the photocatalytic behavior is influenced by various facts, and it is difficult to draw unifying conclusion by direct comparisons between the studies, including particle size, surface area, crystallinity, state of surface hydration, concentration of catalysts and doped ions [29–32]. Various synthetic techniques have been developed to obtain uniform size and high crystallinity dopants with big surface areas. It is known that the gel process leads to the greatest possible homogeneous distribution of the dopant in the host matrix and high surface area of TiO_2 particles among various synthetic routes [33–35] and the hydrothermal method is readily to obtain uniform size nanocrystal [34].

In the present work, gel and hydrothermal techniques were combined to prepare homogeneously distributable nanocrystalline Sb_2S_3/Bi_2S_3 doped TiO_2 with coordination compounds $[M(S_2CNEt)_3]$ (M=Sb, Bi; S_2CNEt=pyrrolidinedithiocarbamate) as precursors. $M(S_2CNEt)_3$ was chosen as the precursor because it could form homogeneous gel with tetrabutylorthotitanate (TBOT) and facilely thermodecomposed into Sb and Bi sulfureted doped TiO_2. As-prepared nanopowders Sb and Bi sulfureted doped TiO_2 were characterized by XRD, SEM, UV–vis and XPS. The photocatalytic behaviors of the resulting powders were characterized by the degradation of an organic dye 4-nitrophenol (4-NP) in the aqueous suspension. The detailed microstructural characteristics for the doped TiO_2 systems were investigated based on the doping content and the preparation techniques.

2. Experimental

2.1. Materials

Antimony pyrrolidinedithiocarbamate was synthesized and purified according to literature [36]. All the reagents (AR grade) used in this work were purchased from commercial suppliers without further purification.

* Corresponding authors. Fax: +86 029 88303798.
E-mail addresses: sanpingchen@126.com (S. Chen), gaoshli@nwu.edu.cn (S. Gao).

0022-4596/$ - see front matter © 2010 Elsevier Inc. All rights reserved.
doi:10.1016/j.jssc.2010.12.009

2.2. Characterization

The complex was revealed by X-ray structural analysis. Data were collected for crystals on a Bruker Smart 1000 CCD diffractometer with graphite-monochromated Mo $K\alpha$ radiation ($\lambda = 0.071073$ nm) at 295(2) K. Crystalline phases were revealed by powder X-ray diffraction patterns from a Bruker D8 Diffractometer using a Cu K radiation source ($\lambda = 0.15406$ nm) at a scan rate of 0.03 s/step, operated at 40 kV and 40 mA. The working range was from 20° to 80°. Scanning electron microscopy (SEM) images were performed on a Quanta 400 FEG electron microscopy instrument. Element composition and the chemical state of particle surface were determined by X-ray photoelectron spectroscopy from a Perkin-Elmer Physics Electronics PHI5400X with Al $K\alpha$ radiation source.

Absorption and reflectance spectra of pure and doped semiconductors were recorded by a Shimadzu UV-2550 spectrophotometer equipped with an integrated sphere. $BaSO_4$ was used as a reference to measure all samples. The spectra were recorded at room temperature in air in the range 200–800 nm enabling to study the spectral properties of these materials.

Photocatalytic activity test was carried out in an UV box containing magnetic stirrer. Each reaction suspension was prepared by adding the doped TiO_2 nanopowders (100 mg) into a 100 mL solution mixture of 10^{-4} M 4-nitrophenol in water. The mixture was ultrasonic-treated for 5 min to obtain highly dispersed catalysts. Prior to irradiation, the suspension was magnetically stirred in the dark for

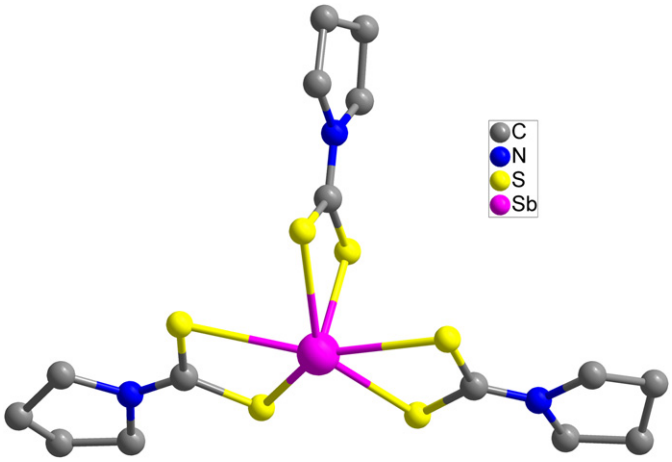

Fig. 1. Molecular structure of Sb complex.

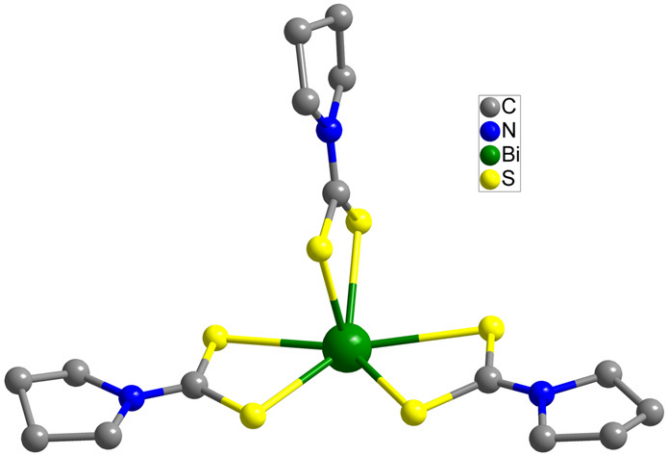

Fig. 2. Molecular structure of Bi complex.

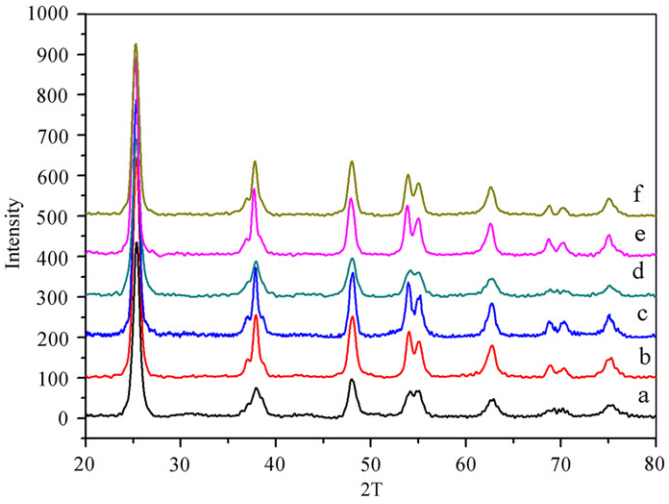

Fig. 3. XRD patterns of doped TiO_2 obtained by different routes. (a) Sb–Ti–1 SG; (b) Sb–Ti–1 SH; (c) Sb_2S_3–Ti–1 GH; (d) Bi_2S_3–Ti–1 SG; (e) Bi_2S_3–Ti–1 SH; (f) Bi_2S_3–Ti–1 GH.

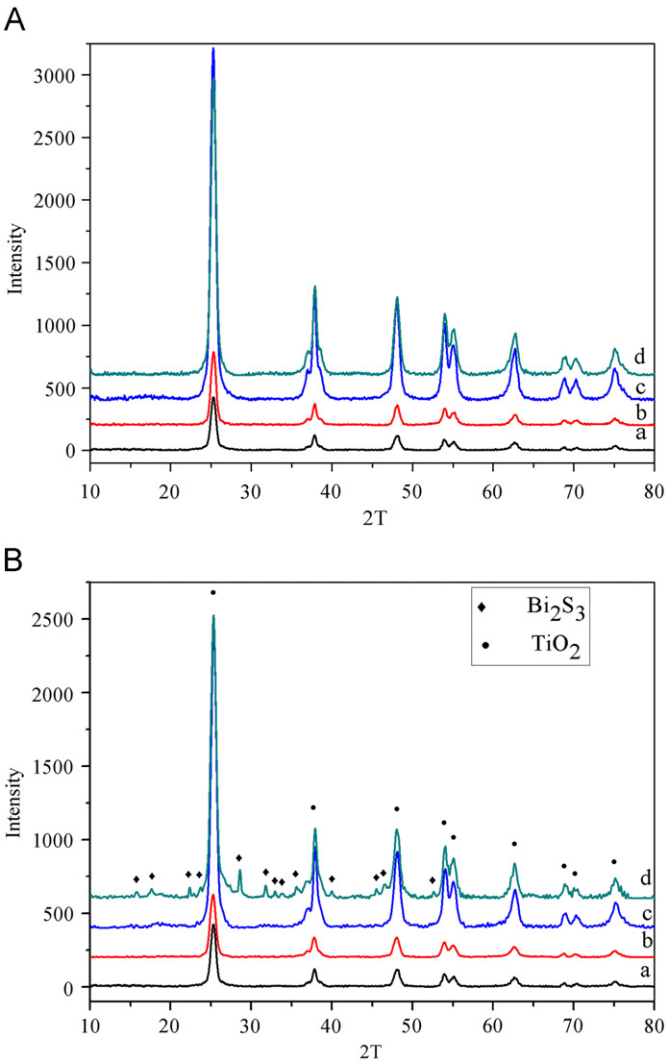

Fig. 4. XRD patterns of Sb_2S_3–Ti–x (A), Bi_2S_3–Ti–x (B) and undoped TiO_2. (A) (a) TiO_2; (b) Sb_2S_3–Ti–1; (c) Sb_2S_3–Ti–3; (d) Sb_2S_3–Ti–5. (B) (a) TiO_2; (b) Bi_2S_3–Ti–1; (c) Bi_2S_3–Ti–3; (d) Bi_2S_3–Ti–5.

30 min to establish adsorption equilibrium. Simultaneously, the suspensions of catalysts in 4-NP were then illuminated using a 250 W Hg UV lamp without bubbling oxygen into the solution. The distance between the liquid surface and light source was about 11 cm. During the photocatalytic testing, the samples were continuously magnetic-stirred. Sampling was performed at the same time intervals for all the samples. The samples (5.0 mL) were taken out and analyzed for 4-nitrophenol concentration by an UV–vis spectrometer (Cary 300). The measure of maximum absorbance was taken at 317 nm.

2.3. Synthesis

Precursor $M(S_2CNEt)_3$ (M=Sb, Bi) preparation: Antimony chloride (6.5 mmol) and tartaric acid (13 mmol) were mixed in an agate mortar and pestled for ca. 15 min during which the ropiness slush was obtained. Upon being adjusted with sodium hydroxide solution and filtered, to which ammonium pyrrolidine dithiocarbamate solution (19.5 mmol) was added drop by drop with constant stirring. Yellow powders as received were then dried and recrystallized from alcoholic solution (ethanol:methanol=1:1) to afford the title complexes. Bismuth complex was obtained similarly as above by using bismuth nitrate instead of antimony chloride and mannitol instead of tartaric acid and recrystallized from the mixture solution (ethanol:N,N-dimethylformamide=1:1).

Doped TiO_2 preparation: A stoichiometric amount of Sb/Bi complex was dissolved in a solution of $Ti(O–Bu)_4$(TBOT) (0.025 mmol) and isopropanol (33.960 mmol), kept stirring at ambient temperature for 30 min. The resulting solution was signed as A. Ice acetic acid (0.098 mol) was dissolved in a solution of isopropanol (0.065 mol) and distilled H_2O (0.111 mol), continuously stirred at ambient temperature for 30 min to get the solution B. B was slowly trickled into A when stirring lasted 1 h at room temperature. The resulting yellow sol with pH value of 3–4, was aged at room temperature for 24 h to form a transparent gel.

Synthesis of SH sample: The sol was transferred to a Teflon-lined autoclave for a hydrothermal treatment at 160 °C for 60 h. The powders signed as SH (sol–hydrothermal) were obtained which subjected to the calcination for 4 h at 500 °C in a nitrogen atmosphere in a furnace with a heating rate of 2 °C/min.

Synthesis of SG sample: The gel (10.3 g) obtained from the sol was dried at 60 °C for 12 h to remove the solvents and the dried gel was calcined at the same condition as SH sample.

Synthesis of GH sample: The gel (10.3 g) was dissolved in distilled H_2O (28.0 ml) by ultrasonic dispersion for 10 min to get a yellow suspension, which was transferred to a Teflon-lined autoclave for a hydrothermal treatment at 160 °C for 60 h. GH (gel–hydrothermal) sample was obtained which subjected to the calcination as same as SH sample. The obtained photocatalysts were denoted as M_2S_3–Ti–x, where M is for the doped metal and x for the doped molar ratio.

3. Results and discussion

3.1. Analysis of crystal structure and chemical composition of doped TiO_2

The compounds $Sb(S_2CNEt)_3$ and $Bi(S_2CNEt)_3$ have isomorphous structures (Figs. 1 and 2), and can be described as pentagonal pyramidal geometries. In the structures, three pyrrolidinedithiocarbamate molecules are asymmetrically chelated to the central metal atom, in which the two pyrrolidinedithiocarbamate ligands are nearly coplanar while the third ligand is approximately orthogonal to the ligands at the apex of the pyramid.

Fig. 3 shows the XRD patterns of TiO_2 powders doped with 1.0 mol% Sb_2S_3 or Bi_2S_3 obtained by various synthetic routes. It reveals that the samples are in single phase with good crystallinity and all peaks are assigned to the anatase phase (tetragonal, $I4_1/amd$, JCPDS 21-1272), no significant diffraction peak of Sb/Bi

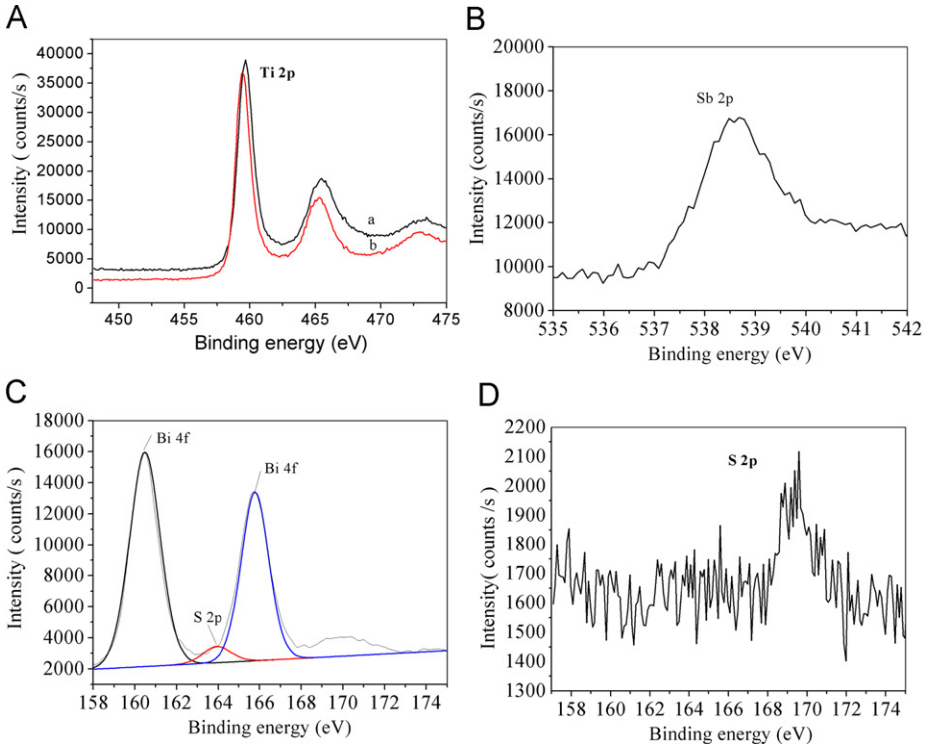

Fig. 5. XPS results of Sb_2S_3–Ti–5 and Bi_2S_3–Ti–3. (A) The Ti 2*p* XPS profiles of Sb_2S_3 (curve b) and Bi_2S_3 (curve a) doped TiO_2. (B) The Sb 3*d* XPS profiles of Sb_2S_3 doped TiO_2. (C) The Bi 4*f* and S 2*p* XPS profiles of Bi_2S_3 doped TiO_2. (D) The S 2*p* XPS profiles of Sb_2S_3 doped TiO_2.

species is observed in each pattern because of the higher dispersion of doped ions and the lower content of Sb_2S_3/Bi_2S_3. The powders synthesized by the GH route show better crystallinity.

Figs. 4 and 5 show the XRD patterns of undoped TiO_2 and M_2S_3 doped TiO_2 prepared by gel–hydrothermal route with different doping ratios. Clearly, the doping of Sb_2S_3/Bi_2S_3 does not affect the crystal phases of photocatalysts. In addition, at low concentration of Bi_2S_3, the presence of Bi_2S_3 is not detected significantly by XRD analysis. At concentration of 5.0 mol%, different peaks attributed to Bi_2S_3 (JCPDS card file no. 17-320) are observed. The presence of Sb_2S_3 is not detected by XRD analysis regardless of the concentration of Sb_2S_3, indicating that Sb_2S_3 is highly dispersed. With increasing the doping ratio from 1.0 to 5.0 mol%, the diffraction peaks become sharp, suggesting an increase of crystallinity. The average crystal size of the particle is estimated from the widths of anatase (101) reflection by the Scherrer formula, $L=0.89\lambda/\beta\cos\theta$, where λ (1.5406 Å) is the wavelength, θ is the Bragg angle (deg.), L is the average crystallite size (nm) and β is the full width at half-maximum. The calculated data indicates that the average crystal sizes for samples are all approximately 12 nm. These results support that the current doping procedure allows stable and uniform mixing dopants.

To determine the surface chemical state of M_2S_3, XPS was used to study the samples as shown in Fig. 5. According to the deconvolution results, the Ti 2*p* spectrum of the M_2S_3 doped TiO_2 dominates by species in the Ti^{4+} oxidation state (Fig. 5A). The binding energy of the Ti 2*p* band in the case of Bi_2S_3 doped TiO_2 samples (Fig. 5A curve a) is found to be a little higher than that of the Sb_2S_3 dopants (Fig. 5A curve b). The peak at 160.8 eV corresponds to the S 2*p* binding energy and the peak at 538.6 eV corresponds to Sb 3*d* binding energy (Fig. 5B and D). The results are in agreement with the reported values of Sb_2S_3 in literatures

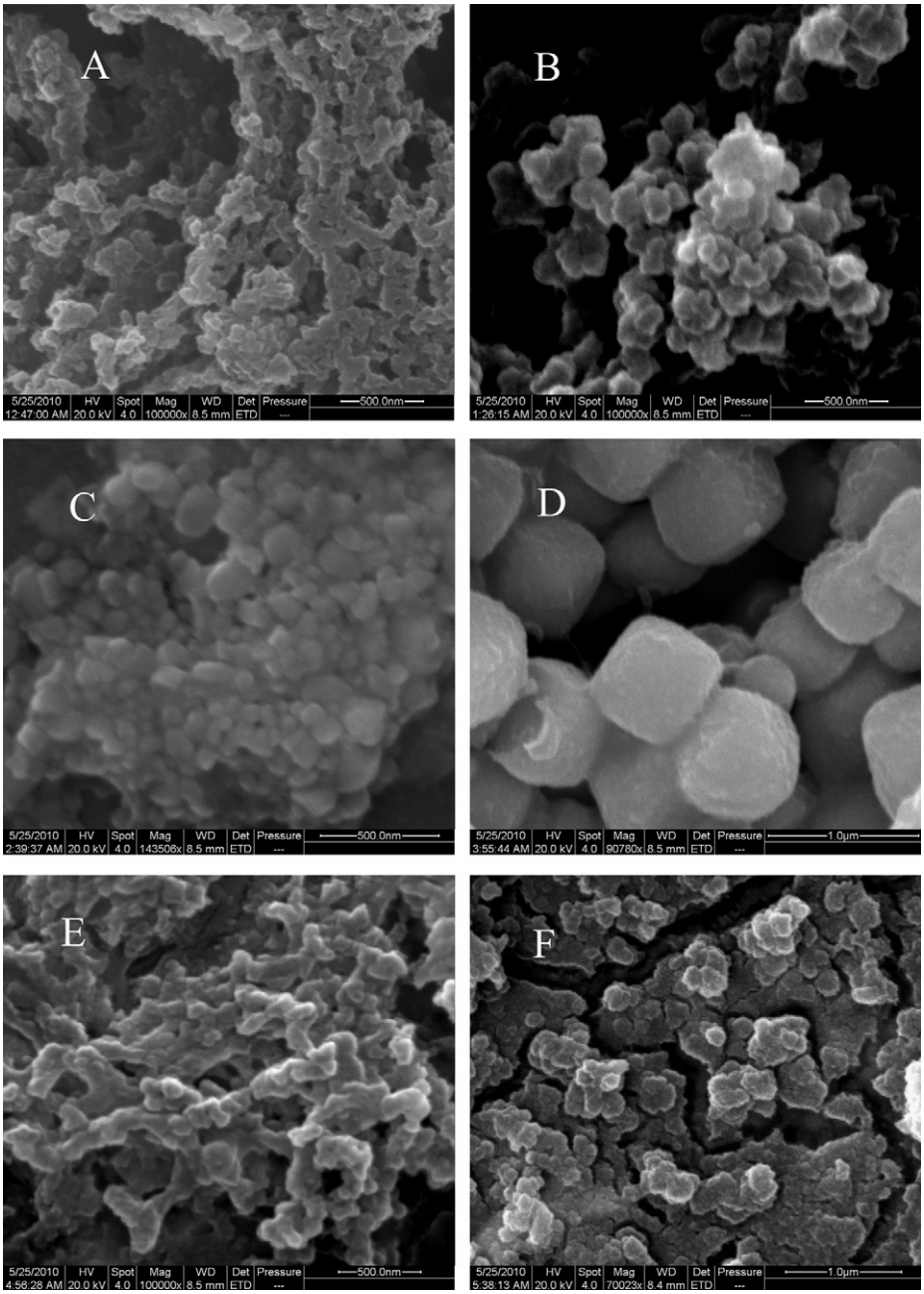

Fig. 6. SEM images of the TiO_2 dopants. (A) TiO_2 G-H; (B) Sb_2S_3–Ti–1 GH; (C) Bi_2S_3–Ti–1 GH; (D) Bi_2S_3–Ti–5 GH; (E) Sb_2S_3–Ti–1 SG; (F) Bi_2S_3–Ti–1 SG.

[37,38]. The peak areas of Sb 3*d*, S 2*p* and Ti 2*p* are quantified to give a molar ratio of Sb:S:Ti of 0.99:1.62:19.44, which is nearly consistent with the anticipated value 1:1.50:20.00 (Sb_2S_3–Ti–5). The two strong peaks in Fig. 5C at 158.5 eV and 163.7 eV correspond to the Bi (4*f*) transitions and the peak at 163.83 eV can be attributed to the S (2 s) binding energy. Quantification of the XPS peaks gives the atomic ratio of Bi:S:Ti as 3.09:1.89:27.21, which is out of the anticipated value 3:4.5:100 (Bi_2S_3–Ti–3). The error probably caused by (1) the error of the simulation and (2) the reductive reaction from Bi^{3+} to trace Bi^0 attributable to the remaining carbonaceous species from the calcination.

Typical SEM images of the TiO_2 dopants are illustrated in Fig. 6. Sb_2S_3 doped TiO_2 particles appear as sphere-like morphology with diameter in the range of 80 nm and Bi_2S_3 doped TiO_2 powders show cubic morphology with diameter in the range of 60 nm as shown in Fig. 6C in which the doped ratio is 1.0 mol%.

Comparing with sol–gel route, GH route avoids abundant agglomeration, as evidenced by Fig. 6B, D, E and F. Different from those of SG route, the particulates from GH route highly disperse and the dopants is a uniform system. A reasonable mechanism may be presumed as that, TBOT is firstly hydrolyzed to produce the gel, which acts with the complex to form a mixing and homogeneous 3D network. Upon hydrothermal process [39], the homogeneous system of gel-complex is then transformed to a uniform doping configuration. Additional, size of particulates increases with increasing the doped ratio, as shown in Fig. 6C and D.

3.2. UV–vis diffuse reflectance spectroscopy

The UV–vis absorption spectra of Sb_2S_3 and Bi_2S_3 doped TiO_2 with different doped molar ratios are illustrated in Figs. 7 and 8, respectively. The Sb_2S_3 doped samples show the weaker absorption intensity than Bi_2S_3 dopants in the visible region of 400–750 nm. As for Bi_2S_3 dopants, absorption intensity increases with increasing doped molar ratio in the region of 550–700 nm which is consistent with reported work [27].

3.3. Photocatalytic activity for photodecolorization of 4-nitrophenol

The photocatalytic properties for the samples are tested on 4-nitrophenol (4-NP) decolorization. Degradation of 4-NP is observed as function of concentration change under UV–vis light. As shown in Fig. 9, the contamination is decomposed completely in the end. In the dark, there is no obvious absorption of 4-NP on the surface of bare or doped TiO_2, suggesting that absorption is not the precondition in the degradation process of 4-NP in this system. Fig. 10 shows

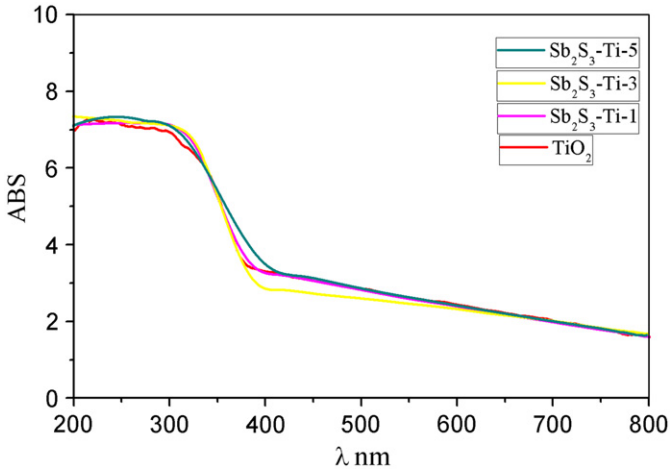

Fig. 7. Diffuse reflectance UV–vis spectra of Sb_2S_3 modified TiO_2.

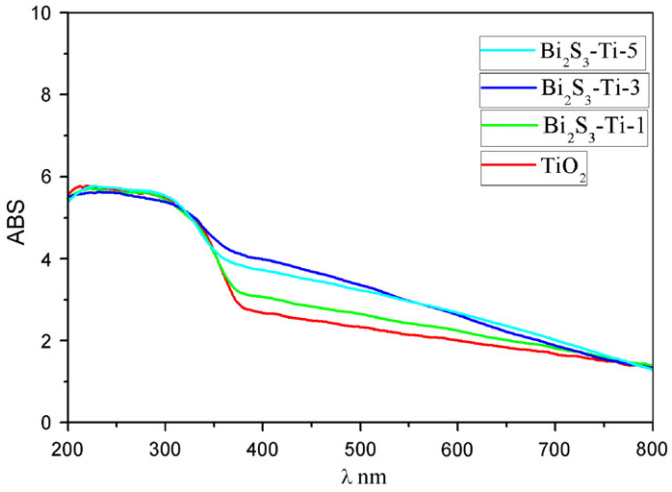

Fig. 8. Diffuse reflectance UV–vis spectra of Bi_2S_3 modified TiO_2.

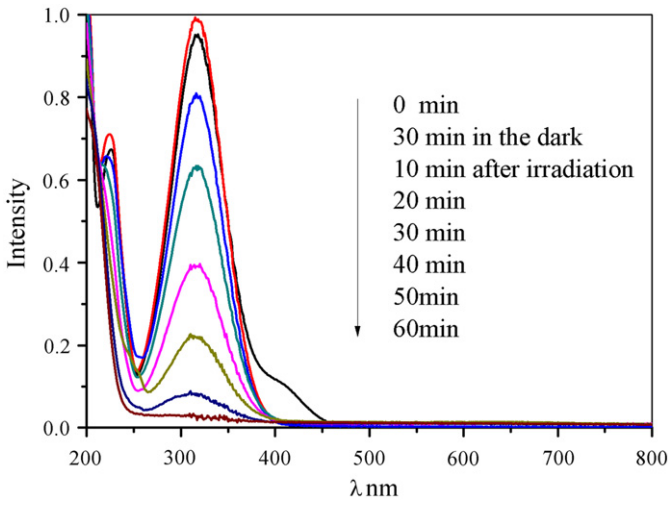

Fig. 9. UV–vis absorption spectra of 4-nitrophenol degraded by Bi_2S_3–Ti–1 catalyst and taken after UV–vis irradiation at intervals of 10 min.

photocatalytic efficiency of Bi_2S_3 or Sb_2S_3 doped TiO_2 versus degradation of 4-NP at different conditions. In contrast with Sb_2S_3 doped TiO_2, Bi_2S_3 doped TiO_2 exhibits better photocatalytic activity, which depends on Bi_2S_3 narrower band gap. The dopants obtained from GH route perform better photocatalytic activity than those SG or SH process. It could be observed that the photocatalytic efficiencies decrease when increasing the amount of Bi_2S_3, as shown in Fig. 11. The same trend has been investigated in literature [27]. This fact is believed to be a consequence of charge carrier dissipations by trapping when the amount of Bi_2S_3 reaches a critical concentration, the critical concentrations of Sb_2S_3 and Bi_2S_3 doped TiO_2 are 3.0 and 1.0 mol%, respectively.

Effect of diverse pH values on the Bi_2S_3–Ti–1 degrading system has been investigated, as shown in Fig. 12. The plots of $\ln(C_0/C)$ versus time for pH result in a straight line. The photocatalytic decolorization of 4-NP is a pseudo-first-order reaction and its kinetics equation can be expressed as $\ln(C_0/C)=kt$, where k is the apparent reaction rate constant, C_0 is the initial concentration of aqueous 4-NP, t is the reaction time and C is the concentration of aqueous 4-NP at the reaction time of t. The apparent rate constants of various pH values are summarized in Table 1. The data given in Fig. 12 show no clear trend because 4-NP is slowly degraded initially

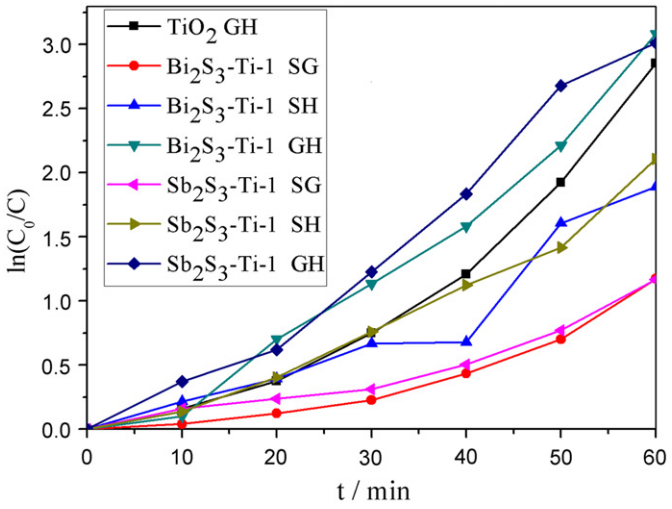

Fig. 10. Photocatalytic degradation of 4-NP using Bi_2S_3 and Sb_2S_3 sensitized TiO_2 obtained by different techniques under UV–vis irradiation.

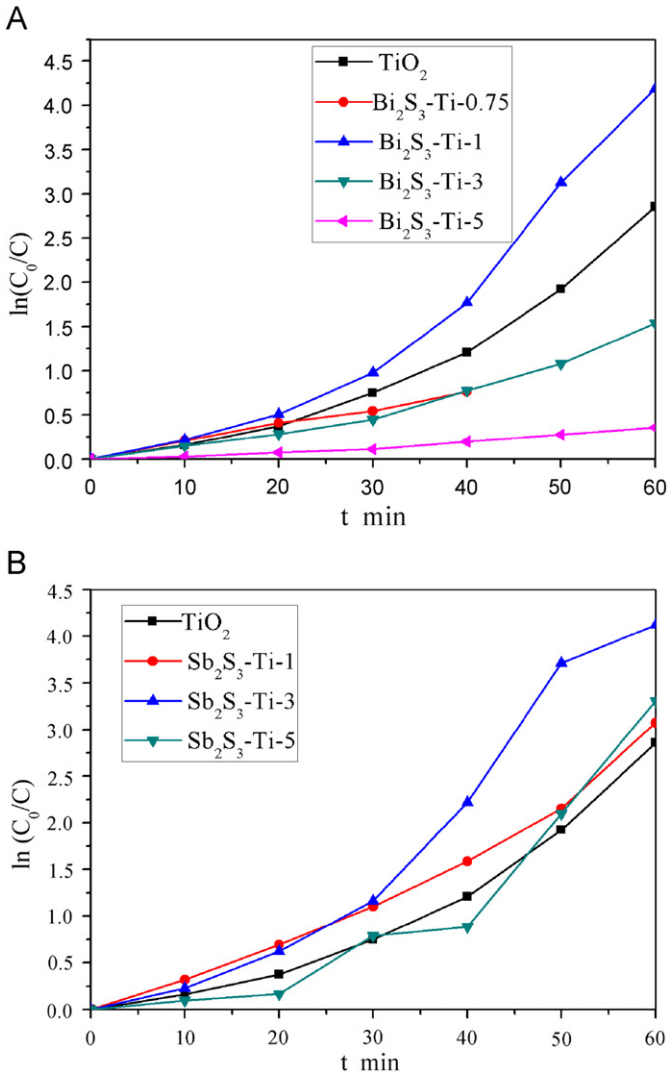

Fig. 11. The plots of $\ln(C_0/C)$ versus time for the amount of Bi_2S_3 and Sb_2S_3 increasing from 1.0 to 5 mol%.

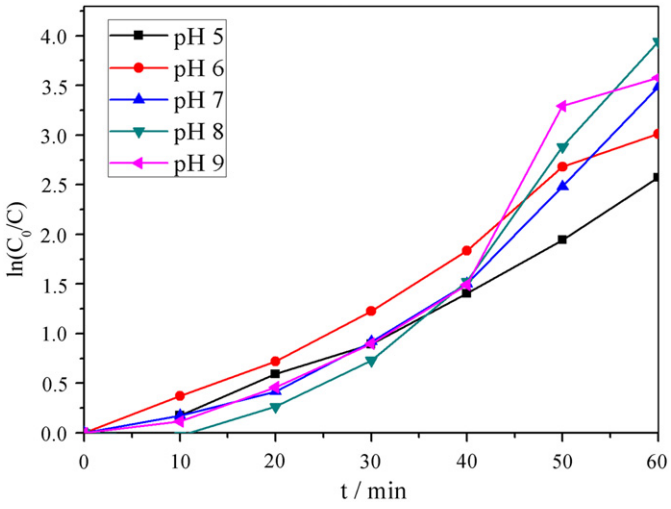

Fig. 12. The plots of $\ln(C_0/C)$ versus time for pHs from 5 to 9.

Table 1
Comparison of the apparent reaction rate constants calculated from Fig. 12 for various pH values when the concentration of catalyst is 1 g/L.

pH	5	6	7	8	9
Apparent reaction rate constant (min^{-1})	0.04309	0.05309	0.05927	0.08140	0.07701

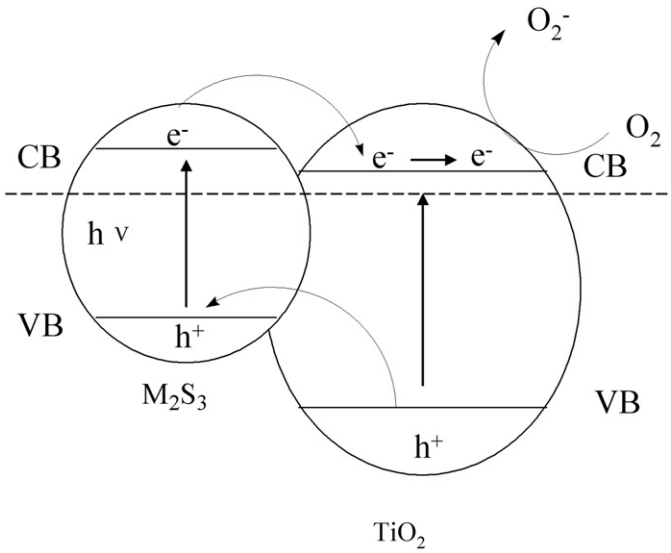

Fig. 13. Energetic diagrams of M_2S_3/TiO_2 system.

compared with the last 30 min when the pH increases. Obviously, the rate of 4-NP decomposition is the fastest at pH 8 from Table 1.

3.4. Mechanism proposal

Using two such semiconductors in contact has a beneficial role in improving charge separation and extands TiO_2 in response to visible light, such as Si_2S_3 ($E_g \sim 1.7$ eV)/TiO_2 and Bi_2S_3 ($E_g \sim 1.3$ eV)/TiO_2 systems. The conduction band of TiO_2 is more anodic than Si_2S_3 and Bi_2S_3, the interparticle electron transfer between colloid Si_2S_3 or Bi_2S_3 and TiO_2 semiconductor system was investigated [27,40]. Based on the reported works [41–43], a mechanism for the degradation of pollutants is proposed as shown in Fig. 13. When the system

is under UV–vis irradiation, Si_2S_3, Bi_2S_3 and TiO_2 are all excited, electrons are injected from the M_2S_3 (M=Sb, Bi) to TiO_2 (Eqs. (1) and (2)) and then scavenged by molecular oxygen O_2 to yield the superoxide radical anion O_2^- (Eq. (3)) and hydrogen peroxide H_2O_2 (Eq. (4)) in oxygen-equilibrated media. These new formed intermediates can interact to produce hydroxyl radical $OH^\bullet$ (Eq. (5)) which is a powerful oxidizing agent capable of degrading most pollutants (Eq. (6)). Holes generated on TiO_2 valence band are transferred to the valence band of M_2S_3. However, the photogenerated holes in M_2S_3 cannot oxidize hydroxyl groups to hydroxyl radicals due to its valence band potential. This results in the photocorrosion of M_2S_3 and an approach is still pursued to make them stable, such as coupled with stable photocatalyst or immersed in solutions of X^{2-} [26,27,44] and so on.

$$M_2S_3-TiO_2 \xrightarrow{h\nu} M_2S_3(e^-+h^+)-TiO_2 \quad (1)$$

$$M_2S_3(e^-+h^+)-TiO_2 \rightarrow M_2S_3(h^+)-TiO_2(e^-) \quad (2)$$

$$e^-+O_2 \rightarrow O_2^{-\bullet} \quad (3)$$

$$2e^-+O_2+2H^+ \rightarrow H_2O_2 \quad (4)$$

$$H_2O_2+O_2^{-\bullet} \rightarrow OH^\bullet+OH^-+O_2 \quad (5)$$

$$OH^\bullet+4NP \rightarrow \text{degradation products} \quad (6)$$

4. Conclusions

Sb_2S_3/Bi_2S_3 doped TiO_2 were prepared with the coordination compounds [$M(S_2CNEt)_3$] (M=Sb, Bi; S_2CNEt=pyrrolidinedithiocarbamate) as precursors via gel–hydrothermal techniques. XRD and SEM analyses demonstrate that higher crystallinity and uniform Sb_2S_3 and Bi_2S_3 doped TiO_2 have been obtained by GH route. Photocatalytic activity of dopants demonstrates the doped TiO_2 powders show much higher rate of photodegradation reaction of 4-nitrophenol (4-NP) compared with bare TiO_2 under UV–vis illumination. Results of 4-NP decolorization indicate that the optimal doped technique is GH route, the optimal Bi_2S_3 and Sb_2S_3 content are 1.0 and 3.0 mol%, respectively, and the optimal pH is 8.

Acknowledgments

We gratefully acknowledge the financial support from the National Natural Science Foundation of China (Grant nos. 20771089, 20873100 and 21073142), the Nature Science Foundation of Shaanxi Province (Grant no. SJ08B09) and the Key Laboratory Foundation of the Education Committee of Shaanxi Province (Grant no. 09JS089).

References

[1] M. Anpo, M. Takeuchi, J. Catal. 216 (2003) 505.
[2] F.-Z. Huang, M.-F. Zhou, Y.-B. Cheng, R.A. Caruso, Chem. Mater. 18 (2006) 5835.
[3] X.-D. Wang, D.R.G. Mitchell, K. Prince, A.J. Atanacio, R.A. Caruso, Chem. Mater. 20 (2008) 3917.
[4] R. Asahi, T. Morikawa, T. Ohwaki, K. Aoki, Y. Taga, Science 293 (2001) 269.
[5] E. Martínez-Ferrero, Y. Sakatani, C. Boissière, D. Grosso, A. Fuertes, J. Fraxedas, C. Sanchez, Adv. Funct. Mater. 17 (2007) 3348.
[6] S. Livraghi, M.C. Paganini, E. Giamello, A. Selloni, C.D. Valentin, G. Pacchioni, J. Am. Chem. Soc. 128 (2006) 15666.
[7] G. Liu, L.-Z. Wang, C.-H. Sun, Z.-G. Chen, X.-X. Yan, L.-N. Cheng, H.-M. Cheng, G.-Q. Lu, Chem. Commun. 11 (2009) 1383.
[8] G. Liu, F. Li, Z.-G. Chen, G.-Q. Lu, H.-M. Cheng, J. Solid State Chem. 179 (2006) 331.
[9] G. Liu, F. Li, D.-W. Wang, D.-M. Tang, C. Liu, X.-L. Ma, G.-Q. Lu, H.-M. Cheng, Nanotechnology 19 (2008) 025606.
[10] G. Liu, X.-W. Wang, L.-Z. Wang, Z.-G. Chen, F. Li, G.-Q. Lu, H.-M. Cheng, J. Colloid Interface Sci. 334 (2009) 171.
[11] S.U.M. Khan, M. Al-Shahry, B. William, Ingler Jr., Sci. 297 (2002) 2243.
[12] S. Sakthivel, H. Kisch, Angew. Chem. Int. Ed. 42 (2003) 4908.
[13] T. Umebayashi, T. Yamaki, H. Itoh, K. Asai, Appl. Phys. Lett. 81 (2002) 454.
[14] W. Zhao, W.-H. Ma, C.-C. Chen, J.-C. Zhao, Z.-G. Shuai, J. Am. Chem. Soc. 126 (2004) 4782.
[15] W. Ho, J.-C. Yu, S. Lee, Chem. Commun. 10 (2006) 1115.
[16] X.-T. Hong, Z.-P. Wang, W.-M. Cai, F. Lu, J. Zhang, Y.-Z. Yang, N. Ma, Y.-J. Liu, Chem. Mater. 17 (2005) 1548.
[17] H. Irie, Y. Watanabe, K. Hashimoto, J. Phys. Chem. B 107 (2003) 5483.
[18] Y.-Q. Wu, G.X. Lu, S.-B. Li, J. Phys. Chem. C 113 (2009) 9950.
[19] Q. Xiao, Z.-C. Si, Z.-M. Yu, G.-Z. Qiu, Mater. Sci. Eng. B 137 (2007) 189.
[20] P. Romero-Gomez, V. Rico, A. Borras, A. Barranco, J.P. Espinos, J. Cotrino, A.R. Gonzalez-Elipe, J. Phys. Chem. C 113 (2009) 13341.
[21] S. Ghasemia, S. Rahimnejada, S. Rahman Setayesha, S. Rohanib, M.R. Gholamia, J. Hazard. Mater. 172 (2009) 1573.
[22] W.-F. Yao, H. Wang, X.-H. Xu, X.-F. Cheng, J. Huang, S.-X. Shang, X.-N. Yang, M. Wang, Appl. Catal. A: Gen. 243 (2003) 185.
[23] W.-F. Yao, X.-H. Xu, H. Wang, J.-T. Zhou, X.-N. Yang, Y. Zhang, S.-X. Shang, B.-B. Huang, Appl. Catal. B: Environ. 52 (2004) 109.
[24] W.-F. Yao, H. Wang, X.-H. Xu, J.-T. Zhou, X.-N. Yang, Y. Zhang, S.-X. Shang, Appl. Catal. A: Gen. 259 (2004) 29.
[25] N. Thanabodeekij, E. Gulari, S. Wongkasemjit, Powder Technol. 160 (2005) 203.
[26] R. Brahimi, Y. Bessekhouad, A. Bouguelia, M. Trari, Catal. Today 122 (2007) 62.
[27] Y. Bessekhouad, D. Robert, J.V. Weber, J. Photochem. Photobiol. A:Chem. 163 (2004) 569.
[28] K.-Q. Li, et al., Chin. J. Synth. Chem. 15 (2007) z1.
[29] G.P. Fotou, S. Vemury, S.E. Pratsinis, Chem. Ing. Sci. 49 (1994) 4939.
[30] C.-K. Chan, J.F. Porter, Y.-G. Li, W. Guo, C.-M. Chan, J. Am. Ceram. Soc. 82 (1999) 566.
[31] A.P. Rivera, K. Tanaka, T. Hisanaga, Appl. Catal. B 3 (1993) 37.
[32] N. Thanabodeekij a, E. Gulari b, S. Wongkasemjita, Powder Technol. 160 (2005) 203.
[33] X.-P. Zhao, J.-B. Yin, Chem. Mater. 14 (2002) 2258.
[34] H.-G. Yang, G. Liu, S.-Z. Qiao, C.-H. Sun, Y.-G. Jin, S.-C. Smith, J. Zou, H.M. Cheng, G.Q. Lu, J. Am. Chem. Soc. 131 (2009) 4078.
[35] Q. Sun, Y.-C. Fu, J.-W. Liu, A. Auroux, J.Y. Shen, Appl. Catal. A: Gen. 334 (2008) 26.
[36] C.L. Raston, A.H. White, J. Chem. Soc. Dalton Trans. 791 (1976).
[37] Q. Yang, K.-B. Tang, C.-R. Wang, Y.-T. Qian, W.-C. Yu, G.-E. Zhou, F.-Q. Li, J. Mater. Chem. 11 (2001) 257.
[38] C.D. Wagner, W.W. Riggs, L.E. Davis, J.F. Moulder, G.E. Muilenberg, Handbook of X-ray Photoelectron Spectroscopy, Perkin-Elmer Corp., Physical Electronics Division, Eden Prairie, MN, 1979.
[39] G. Xie, Z.-P. Qiao, M.-H. Zeng, X.-M. Chen, S.-L. Gao, Cryst. Growth Des. 4 (2004) 513.
[40] S. Messina, M.T.S. Nair, P.K. Nair, Thin Solid Films 515 (2007) 5777.
[41] M. Kaneko, I. Okura (Eds.), Photocatalysis, Science and Technology, Springer, 2002
[42] M.R. Hoffmann, S.T. Martin, W. Choi, D.W. Bahnemann, Chem. Rev. 95 (1995) 69.
[43] N. Serpone, R.F. Khairutdinov, in: P.V. Kamat, D. Meisel (Eds.), Semiconductor Nanoclusters, Physical, Chemical, and Catalytic Aspects, Elsevier Science, 1997
[44] Y. Itzhaik, O. Niitsoo, M. Page, G. Hodes, J. Phys. Chem. C 113 (2009) 4254.